Lightweight design of the chassis framework for a self-propelled peanut planter in hilly areas based on finite element analysis

Yan Yu, Dazhi Yi, Jiasheng Wang*, Xiaozhi Tan, Xiaomin Wang, Weikang Dong, Yushuai Song
(*College of Mechanical and Electrical Engineering, Qingdao Agricultural University, Qingdao 266109, Shandong, China*)

Abstract: The chassis frame of the self-propelled peanut seeder in hilly and mountainous areas is the main supporting structure of the entire machine, and its weight directly affects the operational performance of the seeder. Therefore, in response to the issues of structural heaviness, strength redundancy, and short endurance of the self-propelled peanut seeder in hilly and mountainous areas, this study aims to reduce the overall weight of the machine, conserve resources, and extend the seeder's endurance time. The research focuses on the chassis frame of the self-propelled peanut seeder, utilizing SolidWorks for 3D modeling. A finite element model of the chassis frame is established using ANSYS Workbench, followed by modal analysis and static analysis under four different working conditions. Based on sensitivity analysis, design variables for the chassis frame are selected, and the response relationships between these design variables are simulated using the Latin Hypercube Design method combined with the Kriging approximation model. Finally, a multi-objective lightweight design is conducted based on the MOGA algorithm. The results indicate that the optimized chassis frame mass is reduced by 28.9%, while meeting the strength requirements. Field tests indicate that the plant spacing qualification rate is ≥98%; the seeding depth operational performance is stable, with an average qualification rate of seeding depth ≥90%. After lightweight design, the prototype structure is stable and the performance is reliable. The research results can provide reference and theoretical basis for the structural optimization and design of the walking chassis frame of self-propelled peanut planters in hilly and mountainous areas.

Keywords: self-propelled peanut planter, chassis framework of the walking platform, multi-objective optimization, lightweight design, finite element analysis
DOI: 10.25165/j.ijabe.20251805.9447

Citation: Yu Y, Yi D Z, Wang J S, Tan X Z, Wang X M, Dong W K, et al. Lightweight design of the chassis framework for a self-propelled peanut planter in hilly areas based on finite element analysis. Int J Agric & Biol Eng, 2025; 18(5): 117–126.

1 Introduction

Peanuts are an important economic and oilseed crop in China[1]. In terms of peanut cultivation, there are many peanut planting areas in the hilly and mountainous regions of our country, with a large distribution in both the north and south[2]. The cultivated land area in hilly and mountainous areas of our country accounts for more than one-third of the national land area. The level of agricultural mechanization in these areas is relatively low, less than 40%. Promoting the mechanization of peanut sowing machines in hilly and mountainous areas can effectively reduce labor intensity[3]. Compared to traditional towed peanut sowing machines, self-propelled sowing machines have advantages such as a smaller turning radius, flexibility, and strong adaptability to slopes[4]. These features can improve the efficiency of peanut sowing in hilly and mountainous areas, reduce labor costs, and accelerate the healthy and sustainable development of the peanut industry in our country.

The overall quality of a self-propelled peanut planter not only affects its operational efficiency but also impacts its energy consumption during operation[5]. The walking chassis, as a key component of the self-propelled peanut planter, serves as the main supporting structure of the entire machine. The fertilizer distributor, seed dispenser, film covering device, and soil covering device must all be installed on the chassis frame[6]. Its quality accounts for a significant proportion of the total weight of the machine, which is crucial for ensuring the working stability and reliability of the self-propelled peanut planter[7]. In addition, the chassis of the walking platform must withstand the impact of the ground and external loads during field operations, requiring sufficient strength and rigidity to prevent deformation and fracture[8]. Given the complex natural and geographical environment of hilly and mountainous areas, the self-propelled peanut planter needs to possess characteristics of compactness, lightweight design, and stable performance[9,10]. Therefore, it is particularly important to carry out a lightweight design of the chassis of the self-propelled peanut planter with the goal of reducing weight, while ensuring the overall operational requirements and structural stability of the machine.

Although lightweight technology has been widely applied in the field of mechanical manufacturing, especially in industries such as aerospace and automotive manufacturing[11], its application in agricultural machinery is still in the early stages. Currently, lightweight design mainly involves three aspects: material selection, manufacturing techniques, and structural improvement and optimization. Among these, structural improvement and

Received date: 2024-10-21 **Accepted date:** 2025-06-04
Biographies: Yan Yu, PhD, Professor, research interests: intelligent agricultural equipment, Email: 83518691@qq.com; **Dazhi Yi**, MS candidate, research interests: agricultural machinery design and control, Email: 2406677654@qq.com; **Xiaozhi Tan**, MS candidate, research interests: agricultural electrification and automation, Email: 384461662@qq.com; **Xiaomin Wang**, MS candidate, research interests: agricultural electrification and automation, Email: 2298014546@qq.com; **Weikang Dong**, MS candidate, research interests: agricultural machinery design and control, Email: 18354673839@163.com; **Yushuai Song**, MS candidate, research interests: agricultural machinery equipment engineering, Email: 1006213566@qq.com.
***Corresponding author: Jiasheng Wang**, PhD, Professor, research interest: agricultural machinery and equipment. College of Electrical and Mechanical Engineering, Qingdao Agricultural University, Qingdao 266109, China. Tel: +86-15854209587, Email: jiasheng0813@163.com.

optimization is one of the key strategies for achieving lightweight chassis. Zhang et al.[12] used ant colony algorithm to optimize the size of TC4 titanium alloy longitudinal beams for light electric commercial vehicle frames, achieving a weight reduction of 15.5% and meeting the requirements of strength and stiffness. Yu et al.[13]conducted a multi-objective structural optimization and lightweight design of the peanut seeder frame based on the SOA algorithm, reducing the frame weight while ensuring its strength. Xu et al.[14] used finite element analysis and multi-objective optimization method based on genetic algorithm to carry out lightweight design of the improved tobacco rod pulling machine frame structure. The optimized frame weight was reduced by 18%, and the prototype vibration characteristics were good. Zhang et al.[15] proposed an improved preference selection index (MPSI) and combined it with multiple methods to optimize the frame of heavy-duty tractors, achieving improvements in lightweighting and fatigue resistance performance, and verifying the reliability and efficiency of MPSI. Li et al.[16] used the dynamic load allowable stress and natural frequency of soybeans as constraints for the soybean harvester frame. The structurally lightweight design is optimized with the goal of minimizing the frame mass. The optimized frame mass is reduced by 16%. Zhang et al.[17] conducted sustainable lightweight design of airport waiting frames based on ANSYS Workbench. Through size and topology optimization, the weight was reduced by 34.8% and the resource utilization rate was improved.

The 2PD-1E self-propelled peanut seeder developed by our research group in hilly and mountainous areas, driven by a crawler chassis, can adapt to complex natural environments and can independently complete fertilization, seeding, ditching, film mulching, and film mulching operations. This paper takes the walking chassis frame of the machine as the research object, aiming at reducing the weight and energy consumption of the frame, constructs the three-dimensional model and finite element optimization model of the chassis frame based on SolidWorks and ANSYS Workbench, and carries out modal analysis and multi-condition static analysis through ANSYS Workbench. After sensitivity analysis and selection of design variables, the MOGA optimization algorithm is used to carry out multi-objective lightweight design of the chassis frame, which provides ideas for lightweight improvement of self-propelled peanut seeders in hilly and mountainous areas.

2 Model establishment of the walking chassis frame

2.1 Establishment of 3D model of frame

The walking chassis frame of the 2PD-1E self-propelled peanut seeder in hilly and mountainous areas is an integrated frame structure, which is welded by rectangular steel pipe and steel plate, and the material is 45MN steel. The supporting part of the electric push rod is made of all metal materials, in which the base, front-end connector, and outer support pipe are made of aluminum alloy, the inner telescopic rod is made of stainless steel, and the motor is made of copper alloy. Before the finite element analysis, SolidWorks 3D drawing software was used to carry out parametric solid modeling for the rack and main parts. The model is shown in Figure 1, and the material parameters of each component are shown in Table 1 and Table 2.

2.2 Establishment of finite element model of frame

In order to improve the analysis effect and obtain a high-precision finite element model, the walking chassis frame is simplified on the premise of ensuring the calculation accuracy. All components of the rack are connected by welding, and the welding relationship is simulated by node coupling and processed as a whole[18,19]; the three-dimensional solid model established by SolidWorks is imported into ANSYS Workbench, and the mesh module is used to divide the mesh (the size is set to 10 mm)[20], 191 870 elements and 636 120 nodes are obtained, and the finite element model is shown in Figure 2.

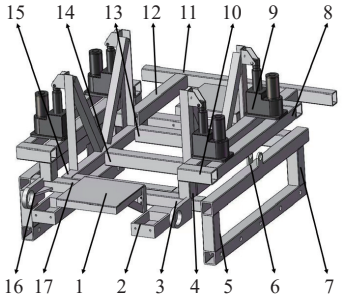

1. Battery support frame 2. Gearbox fixing base 3. Front cross member of lower frame 4. Upper frame pillar 5. Front pillar of chassis lower frame 6. Top beam of lower frame 7. Rear pillar of lower frame 8. Longitudinal beam of upper frame 9. Lifting mechanism 10. Upper frame crossbeam 11. Rear cross member of upper frame 12. Rear longitudinal beam of upper frame 13. Rear cross member is supported in the middle of the upper frame 14. Middle support beam of upper frame 15. Front longitudinal beam of upper frame 16. Transmission shaft fixing plate 17. Front cross member is supported in the middle of the lower frame

Figure 1 3D model of chassis frame

Table 1 Chassis frame material characteristic parameters

Material	Elastic modulus/ MPa	Poisson's ratio	Density/ t·mm^{-1}	Yield strength/ MPa
45Mn Steel	2.05×10^5	0.269	7890	375

Table 2 Material characteristic parameters of lifting device

Material	Elastic modulus/ MPa	Poisson's ratio	Density/ t·mm^{-1}	Yield strength/ MPa
Stainless steel	1.93×10^5	0.31	7750	207
Aluminum alloy	7.1×10^4	0.33	2770	280
Copper alloy	1.1×10^5	0.34	8300	280

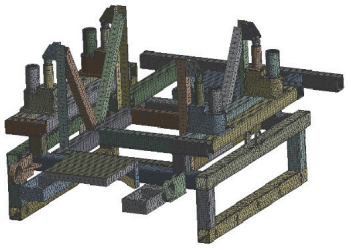

Figure 2 Finite element model of chassis frame

3 Simulation analysis of chassis frame

3.1 Apply load

Static structural analysis was performed on the original chassis, where external loads are the main source of stress in the chassis[21]. The mass parameters of the components of the self-propelled peanut seeder in hilly areas are listed in Table 3. Since the yield strength of 45Mn steel is 375 MPa and taking the safety factor as 1.2[22], the allowable stress of the material is calculated to be 312 MPa according to Equation (1):

$$[\sigma] = \frac{\sigma_s}{n} \quad (1)$$

where, $[\sigma]$ represents allowable stress, MPa; σ_s represents material stress, MPa; and n represents the safety factor.

Table 3 Quality parameters of self-propelled peanut seeder

Component	Quality/kg
Fertilizer box	20
Seed box	15
Fertilizer spreader	2
Seed drill	3
Chassis rack	71
Ditch diggers and other components	60
Motor and reducer	55
Battery	160
Electric push rod support device	6
Under chassis rack	108

3.2 Apply boundary conditions

When conducting finite element analysis on the walking chassis frame of the 2PD-1E self-propelled peanut seeder in hilly and mountainous areas, combined with its field working characteristics, the basic working conditions are determined as bending, torsion, turning, and braking[23]. Considering the complex load borne by the self-propelled seeder in the field, the complex impact load can be simplified as a dynamic load in the actual calculation. Since the dynamic load is often presented in combination, the actual force value is represented by multiplying the static load by the dynamic load coefficient, and the expression of the dynamic load coefficient is:

$$n = 1 + \frac{K_\alpha + K_\beta}{G} \times \frac{C_\alpha}{1 + \frac{C_\beta}{V^2}} \tag{2}$$

where, K_α represents the stiffness of the front wheel spring system, N/m; G is the weight of the self-propelled planter, kg; C_α is the road constant; C_β is an empirical coefficient; and V is the travel speed, km/h.

The working parts of the seeder act vertically on the walking chassis frame in the form of an approximately uniform load. The influence of the road surface and other external impact loads under different working conditions is ignored in the analysis, and the boundary conditions are reasonably added[24]. The traveling chassis frame is defined as the X-axis in the transverse direction, the Y-axis in the vertical direction, and the Z-axis in the longitudinal direction. The boundary conditions under the four working conditions are shown in Table 4.

Table 4 Dynamic load coefficient and boundary conditions

Working conditions	Dynamic load coefficient	Boundary conditions
Bending conditions	2.0	Constrain the support wheels on both the left and right sides as fixed ends
Torsional conditions	2.0	Constrain one side as a fixed end and constrain the support wheels UX and UZ on the other side
Turning conditions	1.3	Constrain the support wheel on one side as a fixed end, constrain the degrees of freedom in the UY and UZ directions on the other side, and apply a centrifugal force of 0.4 g on the turning side
Braking conditions	1.5	Constrain the support wheels on both the left and right sides as fixed ends, and apply an inertial force of -0.6 g in the Y direction

3.3 Static analysis

3.3.1 Bending conditions

The bending condition is a typical scene of the field operation of the self-propelled peanut seeder, which mainly simulates the stress state of the field when it is fully loaded with seeds and fertilizer. The simulation analysis results of the walking chassis frame under this condition are shown in Figure 3.

The simulation results show that the maximum stress is 186.23 MPa, which is mainly concentrated in the connection between the battery support plate and the left and right rods behind the support rod. This value is less than the maximum yield limit of 45MN steel, and there is a large space for lightweight optimization. The maximum displacement of the rack is 0.952 53 mm, which occurs at the connection between the battery support plate and the front of the support rod.

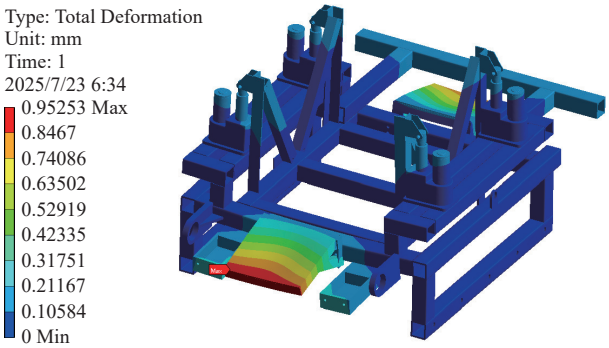

a. Displacement diagram of bending condition

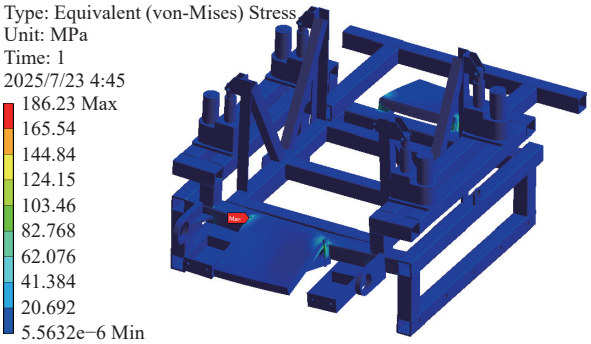

b. Stress diagram of bending condition

Figure 3 Simulation results of frame bending condition

3.3.2 Torsional conditions

The torsion condition simulates the stress state of the frame with the single-side roller suspended during the operation of the seeder. The simulation is carried out for the suspension scene of the right-side roller. The simulation results are shown in Figure 4.

The simulation results show that the maximum stress is 186.19 MPa, mainly acting on the connection between the battery support plate and the left and right rods at the rear of the support rod. This force is less than the maximum yield limit of 45Mn steel and can be optimized for lightweighting. The maximum displacement of the rack is 0.943 82 mm, which occurs at the connection between the battery support plate and the front of the support rod.

3.3.3 Turning conditions

The turning condition mainly simulates the scene of a seeder turning while working in the field. This simulation simulates the vehicle turning to the left. The simulation analysis results of the walking chassis frame under this operating condition are shown in Figure 5.

The simulation results show that the maximum stress is

122.78 MPa, mainly acting on the connection between the battery support plate and the rear of the left and right edges of the support frame. This force is less than the maximum yield limit of 45Mn steel and can further achieve lightweight optimization. The maximum displacement of the rack is 0.699 96 mm, which occurs at the top corner of the right front of the battery support plate and support rod.

3.3.4 Braking conditions

The braking condition mainly simulates the braking scene of the seeder during field operation. This simulation is for emergency shutdown. The simulation analysis results of the walking chassis frame under this condition are shown in Figure 6.

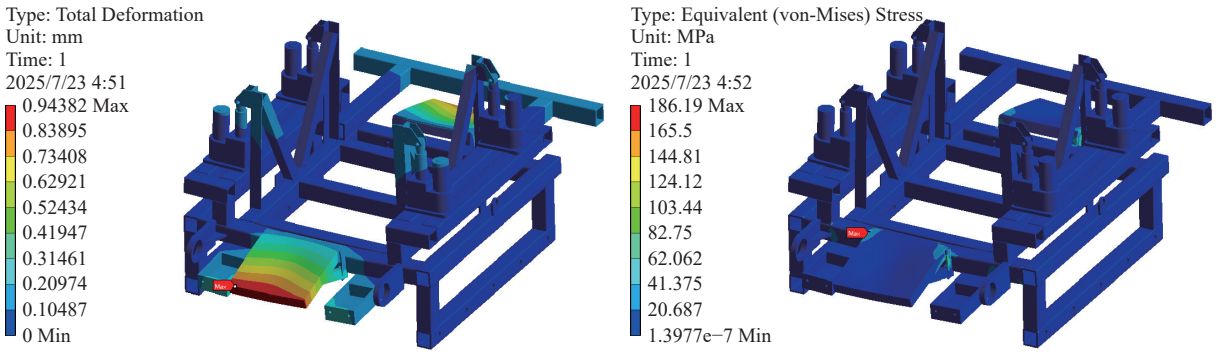

a. Displacement diagram of torsional condition b. Stress diagram of torsional condition

Figure 4 Simulation results of frame torsion condition

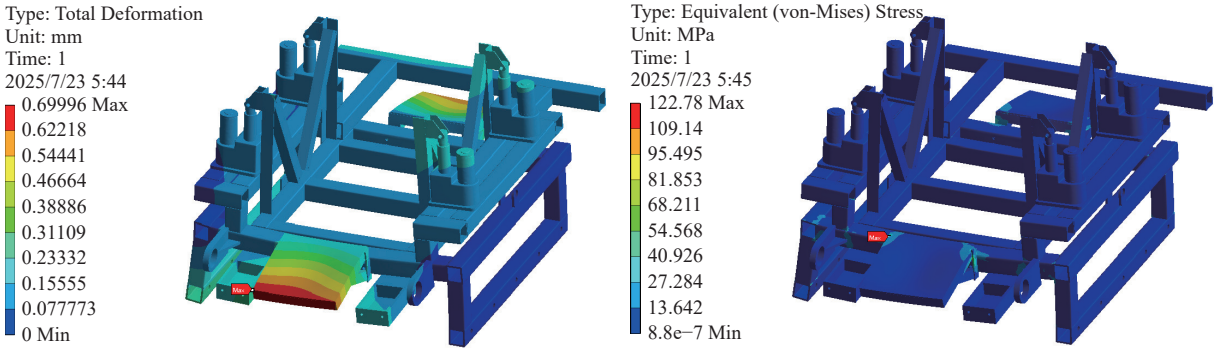

a. Displacement diagram of turning condition b. Stress diagram of turning condition

Figure 5 Simulation results of frame turning condition

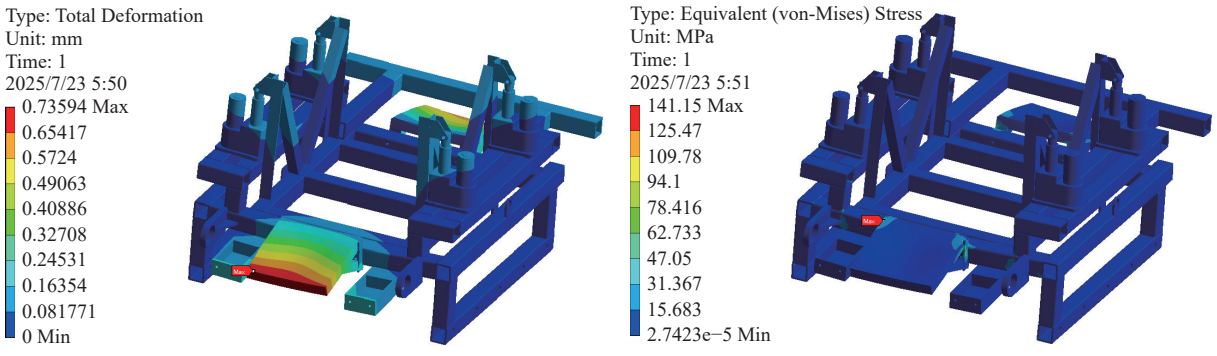

a. Displacement diagram of braking condition b. Stress diagram of braking conditio

Figure 6 Simulation results of frame braking condition

The simulation results show that the maximum stress is 141.15 MPa, mainly acting on the angle between the battery support plate and the connection between the two rods at the right rear of the support rod. This force is less than the maximum yield limit of 45Mn steel and can further achieve lightweight optimization. The maximum displacement of the rack is 0.735 94 mm, which occurs at the edge of the connection between the battery support plate and the front of the support rod.

3.4 Modal analysis

Modal is the inherent vibration characteristic of the structure, and its corresponding modal parameters can reflect the vibration state and characteristics of the structure through superposition[25]. As an important part of structural analysis, modal analysis is the basis for the study of structural dynamic characteristics[26]. As the key bearing component of the whole machine, the walking chassis frame should not only meet the requirements of sufficient structural strength and stiffness but also have good dynamic performance to avoid the frame resonance caused by external excitation frequency excitation during the operation of the self-propelled peanut seeder, which will lead to work failure[27,28].

3.4.1 External excitation frequency analysis

Analyzing the frequencies of different types of excitation sources is helpful to evaluate the dynamic mechanical properties of the chassis frame.

(1) Analysis of excitation frequencies of the motor and rotating components

When all types of motors and rotating components are in operation, the excitation frequency can be calculated based on the rotational speed, using the formula:

$$f = \frac{n}{60} \tag{3}$$

where, n represents the rotational speed, r/min.

Using the above formula, the theoretical excitation frequencies of each drive motor and main rotating component on the chassis frame can be calculated, as summarized in Table 5.

Table 5 Vibration frequency of the excitation source

Excitation source	Rotational speed/r/min	Frequency/Hz
Xinda DC high-speed motor	10 000	166.7
DC servo motor	1500	25
Brushless DC motor	1500	25
Track drive wheel	85.44	1.4

(2) Analysis of road surface excitation frequency

The excitation frequency of road unevenness is:

$$f = \frac{v}{3.6\lambda} \tag{4}$$

where, f is the road surface excitation frequency; v is the forward speed of the seeder, km/h; and λ is the wavelength of the road unevenness, m.

According to the actual rural road conditions, common road surfaces include flat rural roads with wavelengths of 1.0-6.3 m, gravel roads with wavelengths of 0.32-6.3 ms, and unpaved roads with wavelengths of 0.77-2.5 m. The maximum traveling speed of the self-propelled peanut seeder is 3 km/h; therefore, the maximum excitation frequency f_{max} generated by the road surface is

$$f_{max} = 3.6/(3.6 \times 0.32) = 2.60 \text{ Hz}$$

3.4.2 Modal simulation results of the chassis frame

The modal module of ANSYS Workbench is used to carry out modal analysis of the walking chassis frame, and its boundary condition is set as an unconstrained free state during the analysis. The results show that the first six natural frequencies are close to zero and are rigid body modes. Therefore, the natural frequencies of order 7-12 are mainly analyzed. The results are shown in Table 6. From the modal analysis results, it can be seen that the 7-12 natural frequencies of the frame are greater than the external excitation frequencies of the seeder, and there is a certain frequency interval, so resonance will not occur, indicating that its vibration characteristics are reasonable.

Table 6 7-12 order modal frequency of chassis frame

Order	Frequency/Hz
7	77.338
8	81.028
9	99.922
10	126.68
11	131.35
12	143.92

4 Multi-objective optimization design of rack

4.1 Establishment of finite element parametric model

In ANSYS Workbench, the walking chassis frame is divided using shell elements, with the wall thickness, height, and width of each beam treated as design variables for multi-objective optimization. Beams that are symmetrical relative to the central plane of the frame and serve the same function are grouped together. After processing the finite element model, 18 groups of beams and 54 design variables are obtained. The finite element parametric model of the walking chassis frame is shown in Figure 7.

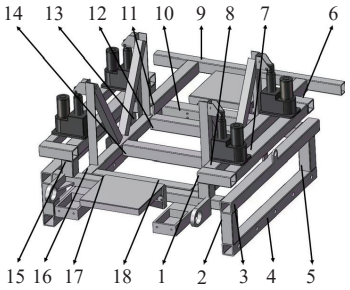

Figure 7 Finite element parametric model of chassis frame

4.2 Parameter selection of design variables

In order to solve the problem that some variables caused by too many design variables have no significant impact on the optimization index, it is necessary to select variables with significant impact for subsequent optimization research[29,30]. Sensitivity analysis can determine the sensitivity of parameter variables to other variables[31], so it is often used to screen design variables in optimization. Taking the total mass, maximum displacement, and maximum stress of the frame as the optimization objectives, the method of combining direct sensitivity with relative sensitivity is used to screen the significant size variables so as to reduce the amount of calculation and improve the calculation accuracy.

This multi-objective optimization design selects the maximum stress and maximum displacement under full-load bending conditions in the static analysis. In ANSYS Workbench, sensitivity analysis is conducted on the chassis frame using the Parameters Correlation module. The design variables include the thickness, height, and width of 18 beams on the chassis frame, resulting in a total of 54 variables. The thickness variables are designated as P1-P54. In the software's parameter settings section, Parameters Set, the initial dimensions for P1-P54 are defined, along with the initial values for the design objectives: mass, maximum displacement, and maximum stress. First, a preliminary screening and merging of the 18 beams is conducted. For example, beams 13, 14, and 18 belong to the same crossbeam, with identical thickness, height, and width. Therefore, P37 and P40 can be replaced by P52; P38 and P41 can be replaced by P53; and P39 and P42 can be replaced by P54. Similarly, the remaining design variables after screening are P1, P2, P3, P4, P5, P6, P10, P11, P12, P13, P14, P15, P16, P17, P18, P19, P20, P21, P22, P23, P24, P25, P26, P27, P28, P29, P30, P31, P32, and P33. The upper and lower limits for the remaining variables are set as listed in Table 7. Set up 100 initial sample points and conduct sensitivity analysis in a nonlinear mode to calculate the sensitivity chart of variables to design objectives, as shown in Figure 8. From Figure 8, it can be seen that P10, P12, P17, and P23 have the most significant impact on the maximum stress, P10 and P12 have the most significant impact on the maximum displacement, and P1, P10, P19, P22, and P31 have the most significant impact on the mass of the walking chassis frame. The core objective of this study is to achieve lightweight design of the walking chassis frame. Therefore, the primary purpose of the design is to reduce weight, while also considering the comprehensive impact of frame

Table 7 Rack design variable value (mm)

Design variable	Initial value	Upper limit	Lower limit
P1	6	6	3
P2	60	60	40
P3	55	55	35
P4	6	6	3
P5	60	60	40
P6	55	55	35
P10	6	6	3
P11	60	60	40
P12	55	55	35
P13	6	6	3
P14	60	60	40
P15	55	55	35
P16	6	6	3
P17	60	60	40
P18	55	55	35
P19	6	6	3
P20	60	60	40
P21	65	70	60
P22	6	6	3
P23	60	60	40
P24	55	55	35
P25	6	6	3
P26	60	60	40
P27	55	5	35
P28	6	6	3
P29	60	60	40
P30	55	55	35
P31	6	6	3
P32	60	60	40
P33	55	55	35

performance parameters. Based on the above analysis, P1, P10, P19, P22, and P31 were ultimately determined as design variables for multi-objective optimization.

4.3 Establishment of the surrogate model

Due to the large number of design variables, this article adopts a Latin hypercube experimental design, selecting a total of 200 experimental sample points.

The Kriging surrogate model is characterized by high sample efficiency in large-scale scenarios, suitability for cases where the variables and objectives are nonlinear, and high global fitting accuracy[32-33]. Therefore, it is suitable for the size optimization problem of the walking chassis frame studied in this paper. The accuracy of the Kriging surrogate model can be tested using the coefficient of determination R^2, expressed as follows:

$$R^2 = \frac{\sum_{i=1}^{h}\left(\hat{y}_1 - \bar{y}\right)^2}{\sum_{i=1}^{b}\left(y_i - y\right)^2} \tag{5}$$

where, h is the number of sample points, y_1 is the predicted value of the surrogate model corresponding to the i^{th} sample point, y_i is the actual response value of the surrogate model corresponding to the i^{th} sample point, and $\bar{y}$ is the average of the actual response values of all sample points.

The coefficient of determination R^2 ranges from 0 to 1, and the closer the value of R^2 is to 1, the closer the model is to the true values. The coefficients of determination for the surrogate models of the walking chassis mass, maximum equivalent stress, and maximum total deformation are all close to 1, as shown in Figure 9. Therefore, the surrogate model is reliable, and the walking chassis frame model has a high fitting accuracy, meeting the design requirements.

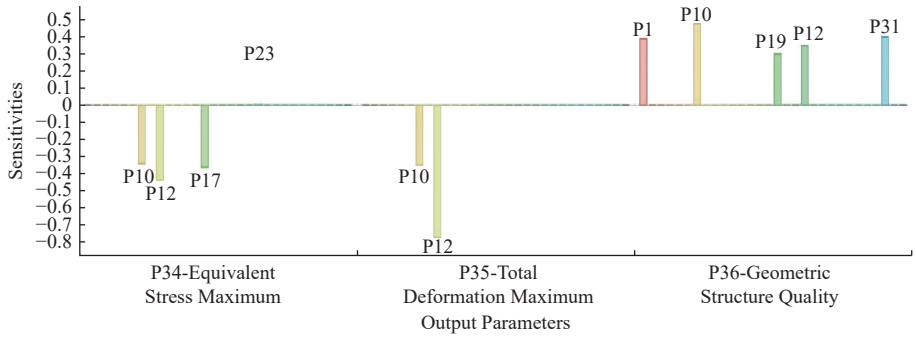

Figure 8 Sensitivity of design variables to maximum displacement, maximum stress, and mass

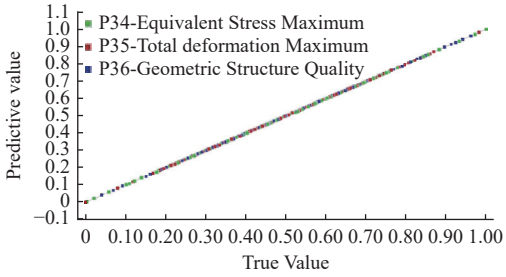

Figure 9 Finite element parametric model of the mobile chassis frame

4.4 Multi-objective optimization of the walking chassis frame based on the MOGA algorithm

The MOGA algorithm was first proposed by Fonseca and Fleming based on genetic algorithms, mimicking the principles of biological evolution by preserving the optimal individuals. The main process of its operation is as follows.

The individual of generation t in the population is defined as:

$$rank(x_i, t) = 1 + P_i^{(t)} \tag{6}$$

where, $rank\ (x_i, t)$ represents the individual order; $P_i^{(t)}$ represents the number of individuals that can be dominated in the t^{th} generation population; x_i represents the specific individual in the t^{th} generation.

When an individual is not dominated within the current generation population, its order is 1. Fitness values are assigned to all individuals using an interpolation function, and sharing ensures that the optimal individuals can be preserved. The flowchart of the MOGA algorithm is shown in Figure 10.

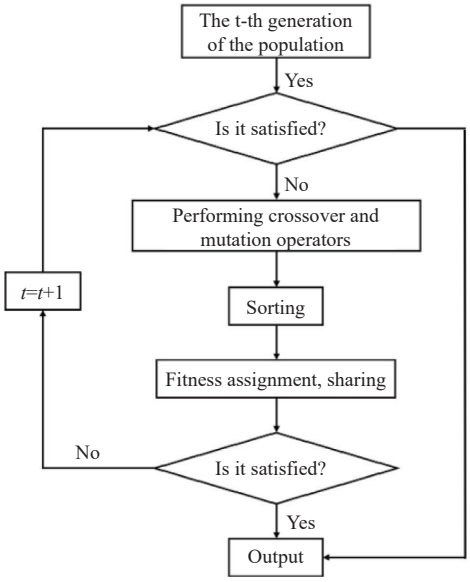

Figure 10 MOGA algorithm flowchart

After a comprehensive analysis of the quality parameters, maximum stress parameters, and maximum deformation displacement parameters of the chassis frame, the final optimization goal is set to minimize weight. Multi-objective optimization is performed on the beam width, beam height, and beam thickness of the walking chassis frame. The optimization mathematical model can be described as follows:

$$\begin{cases} \text{Find}: T=(t_1,t_2,t_3,t_4,t_5,x_1,x_2,x_3,x_4,x_5,h_1,h_2,h_3,h_4,h_5) \\ \text{Min}: M=M(T) \\ \text{Min}: L=L(T) \\ \text{s.t} \begin{cases} 3\ \text{mm} \le t_i \le 6\ \text{mm}, \ i=1,2,3,4,5 \\ 45\ \text{mm} \le x_i \le 55\ \text{mm}, \ i=1,2,3,4,5 \\ 45\ \text{mm} \le h_i \le 60\ \text{mm}, \ i=1,2,3,4,5 \end{cases} \\ \sigma_{\max} \le [\sigma]=312\ \text{Mpa} \end{cases} \quad (7)$$

where, T represents the design variables; $M(T)$ is the total mass of the walking chassis frame; $L(T)$ is the maximum displacement under full load bending conditions of the walking chassis frame; t_i is the thickness of the i^{th} design variable in mm; x_i is the width of the i^{th} design variable in mm; h_i is the height of the i^{th} design variable in mm; σ_{max} is the maximum stress endured by the frame in MPa; and $[\sigma]$ is the allowable stress of the frame in MPa.

After constructing the mathematical model and Kriging model, the MOGA algorithm is used to search for the Pareto optimal solution. The parameters in the MOGA algorithm are set as follows: initial sample points of 4000, iteration times of 100, population size of 100, crossover rate of 0.9, and mutation rate of 0.1. The MOGA algorithm gradually converges to a relatively stable solution and ultimately obtains the optimized Pareto optimal solution, as shown in Figure 11.

The simulation presented a total of 200 sample points in the Pareto frontier, and the sample points with smaller rack mass and maximum rack stress meeting the set conditions were selected as the optimal solution. By optimizing and simulating the rack, sample solutions that meet the optimization objectives and constraints were obtained. The calculated sample points were rounded to obtain the optimized wall thickness, height, and width of the rectangular beam. The rounded values are shown in Table 8.

According to the fourth strength theory, equivalent stress is used as the basis for determining the yield failure stress of materials, and the maximum principal stress is used as an auxiliary criterion. The optimized static structural stress distribution is shown in Figures 12 and 13. After optimization, the equivalent stress and maximum principal stress are still lower than the allowable stress value. According to Tables 9 and 10, the weight of the frame has been reduced by 28.9% from the original 203-144.29 kg after optimization. The modal vibration frequency does not resonate while ensuring the rigidity of the overall frame structure.

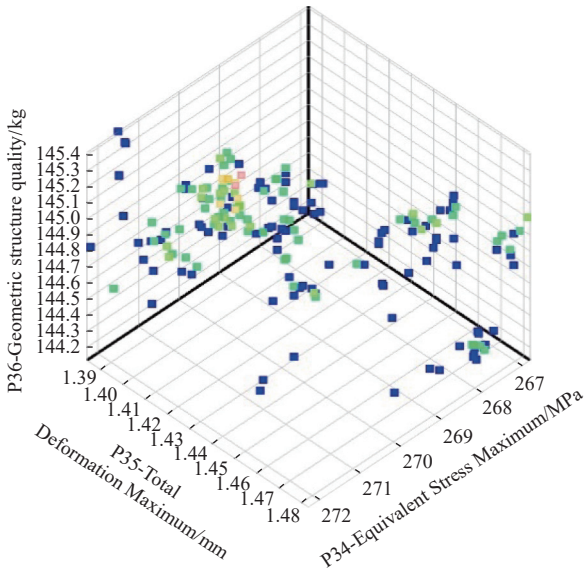

Figure 11 Pareto front diagram

Table 8 Dimension values (rounded) before and after optimization (mm)

Design Variables	Before optimization	Before rounding	After rounding
t_1	6	4.3325	4
t_2	6	4.2356	4
t_3	6	3.9852	4
t_4	6	4.1736	4
t_5	6	4.2245	4
x_1	55	45.1921	45
x_2	55	45.3177	45
x_3	55	45.2567	45
x_4	55	45.4128	45
x_5	55	44.9938	45
h_1	60	45.1411	45
h_2	60	45.3369	45
h_3	60	44.9867	45
h_4	60	45.2568	45
h_5	60	45.1331	45

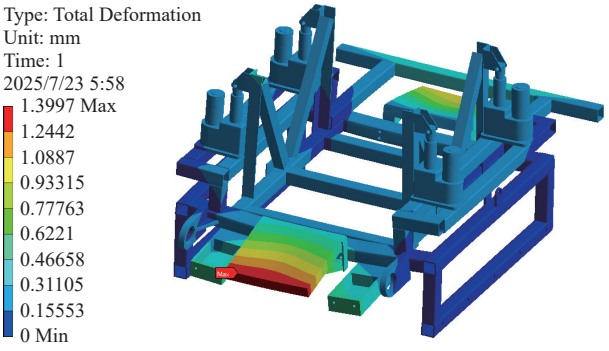

Figure 12 Displacement cloud map of the optimized mobile chassis frame

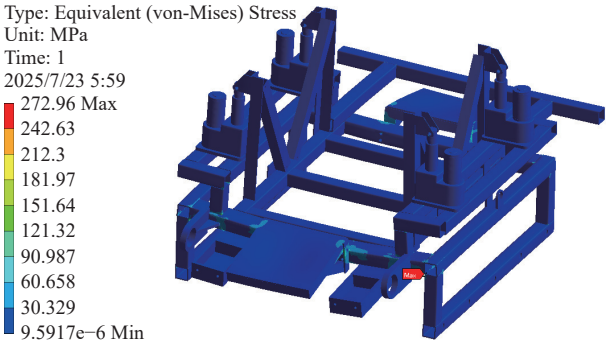

Figure 13 Equivalent stress cloud map of the optimized mobile chassis frame

Table 9 Optimized rear chassis frame parameters

Name	Before optimization	After optimization
Total mass	203 kg	144.29 kg
Maximum deformation	0.952 53 mm	1.3997 mm
Equivalent stress	186.23 MPa	272.96 MPa
Maximum principal stress	136.03 MPa	304.37 MPa

Table 10 Optimized rear chassis frame natural frequency

Order	Frequency/Hz
7	60.08
8	70.263
9	75.624
10	106.51
11	111.37
12	116.36

5 Field tests

To verify the stability and reliability of the walking chassis frame of the self-propelled peanut seeder for hilly areas, Qingdao WanNongDa Peanut Machinery Co., Ltd. completed the processing of the prototype of the 2PD-2E self-propelled peanut seeder. Using the 2PD-2E as the platform, LuHua No. 11 peanut seeds were used for the field sowing experiment conducted in Laixi City, Qingdao (as shown in Figure 14).

Figure 14 Field experiment diagram

Referring to DB34/T 533-2022 (Technical specifications for mechanized peanut sowing operations) and NY/T 3660-2020 (Quality of peanut seeder operations) as evaluation standards, experiments were conducted to assess the impact of sowing speed on the stability of plant spacing, as well as tests for plant spacing, qualification rate, missed sowing rate, and re-sowing rate. The experimental parameters referenced the agronomic requirements for peanut planting in Santai County, Sichuan, and NY/T 3661-2020 (Technical specifications for full mechanization of peanut production). The tests were conducted at traditional planting spacings of 16 cm, 21 cm, and 27 cm, with a working speed generally ranging from 1 to 3 km/h. Two sowing speed levels were set at 1-2 km/h and 2-3 km/h, with a sowing depth of 2-3 cm.

5.1 Testing methods

(1) Experiment on the impact of sowing speed on plant spacing stability

To investigate the impact of sowing machines on plant spacing stability at different sowing speeds, field experiments were conducted with planting distances set at 16, 21, and 27 cm. The operating speeds of the sowing machine were set at two levels: 1-2 km/h and 2-3 km/h. Each experimental group was repeated three times, and 250 sets of data were collected after each trial.

(2) Determination of plant spacing qualification rate, missed sowing rate, and over-sowing rate

To verify the working performance of the self-propelled peanut sowing machine, the machine was set to operate at normal working speeds (≤3 km/h). The sowing speeds were established at two levels: 1-2 km/h and 2-3 km/h, with planting distances set at 16, 21, and 27 cm for field experiments. Each experimental group was repeated three times, collecting 250 sets of experimental data to obtain the average actual planting distance $\bar{L}$ (m), plant spacing qualification index L_q(%), missed sowing rate M(%), and over-sowing rate R(%). The calculation formulas are as follows:

$$\begin{cases} \bar{L} = \dfrac{L}{N_Z} \\ L_q = \dfrac{N_L}{N_Z} \times 100\% \\ M = \dfrac{N_m}{N_Z} \times 100\% \\ R = \dfrac{N_r}{N_Z} \times 100\% \end{cases} \tag{8}$$

where, N_Z represents the total measured quantity, with N_Z=250 in this experiment; L is the measured plant spacing, m; N_L is the number of qualified plant spacings ($0.5L_\alpha \le L \le 1.5L_\alpha$); N_m is the total number of missed seeds ($L > 1.5L_\alpha$); N_r is the number of over-sown seeds ($L < 0.5L_\alpha$); and L_α is the set plant spacing, m.

(3) Determination of sowing depth qualification rate

To verify the seeding depth effectiveness of the seeder, a qualified seeding depth is defined as follows: when the set seeding depth is greater than or equal to 3 cm, an error of ±1 cm is acceptable; when the seeding depth is less than 3 cm, an error of ±0.5 cm is acceptable. The set seeding depth for peanuts is 3 cm, so the allowable error for the seeding depth is set at ±1 cm.

On the working plot, five small areas are randomly selected according to the technical requirements. Each area has a width of one working width and a length of 2 m. The seeding layer is cut open to measure the thickness of the soil covering the seeds. In each area, five points are measured per row. The qualification rate of the seeding depth for each area is calculated and the average value is found. The formula is as follows:

$$H = \frac{h_1}{h_2} \times 100\% \tag{9}$$

where, H represents the qualification rate of the seeding depth, %; h_1 represents the number of qualified points for seeding depth; h_2 represents the total number of measurement points.

5.2 Test results and analysis

(1) Experimental results and analysis of the impact of seeding speed on plant spacing stability

If the seeding spacing is within ±0.5 times the set spacing, it is considered qualified. As shown in Table 11, the seeding effects at 16 cm and 21 cm spacing are better, with qualification rates exceeding 98%. The impact of operational speed on these spacings is minimal. However, at a spacing of 27 cm, the qualification rate is inversely proportional to the operational speed, yet it remains above 96%. This indicates that the seeder maintains a high level of stability at different speeds.

Table 11 Experimental results on the impact of sowing speed on plant spacing stability

Working speed/ km·h^{-1}	Set plant spacing/ cm	Average actual plant spacing/cm			Plant spacing qualification rate/%		
		1	2	3	1	2	3
1-2	16	16.55	16.36	16.07	98.35	98.47	99.01
	21	21.61	21.10	21.23	98.18	98.23	98.45
	27	28.03	26.68	27.19	98.05	98.16	98.27
2-3	16	15.82	16.09	15.77	98.76	98.61	98.83
	21	21.33	20.92	21.23	98.34	98.21	98.39
	27	28.47	27.52	27.89	98.68	96.86	97.87

(2) Experimental results and analysis of plant spacing qualification rate, missed seeding rate, and re-seeding rate

As shown in Table 12, the average qualification rate at the three set spacings and working speeds is 98.19%, with an average missed seeding rate of 1.28%. The seeder has relatively little impact on the qualification rate at medium to low speeds (1-2 km/h and 2-3 km/h), maintaining a qualification rate of around 98%. This indicates that the overall seeding performance is good, and the machine shows good compatibility with the seeder.

Table 12 Field trial performance table of seeders

Working speed/km·h^{-1}	Set plant spacing/cm	Actual plant spacing/cm	Pass rate/%	Missed seeding rate/%	Replay rate/%
1-2	16	16.33	98.61	1.20	0.62
	21	21.31	98.28	1.07	0.93
	27	27.30	98.16	1.36	0.68
2-3	16	15.89	98.73	1.15	0.46
	21	21.16	98.31	1.28	0.30
	27	27.66	97.07	1.66	0.89

(3) Experimental results and analysis of seeding depth qualification rate

The results of the seeding depth qualification rate test for the self-propelled peanut seeder are listed in Table 13. According to NY/T 3660-2020 Peanut Seeder Operating Quality, the qualification rate for seeding depth should be ≥85.0%. Therefore, the parameter value for the seeding depth qualification rate is set at ≥85%. Analysis of the test results indicates that the average seeding depth qualification rate of the seeder is 90%, demonstrating that the self-propelled peanut seeder has relatively stable seeding depth, reliable working performance, and meets agronomic requirements.

The results of the field trials demonstrate that the chassis frame can effectively complete precision seeding operations for peanuts while carrying various working components at different seeding speeds. It is suitable for medium- to low-speed operations in hilly areas and small-scale planting scenarios.

Table 13 Seeding depth qualification rate measurement table

Number of measurement areas	Seeding depth	Number of rows	Measurement point					Pass rate/%
			1	2	3	4	5	
1	2 m/3 cm	1	3.7	3.3	3.6	2.8	3.2	90
		2	3.8	3.2	3.1	1.8	3.5	
2	2 m/3 cm	1	2.7	3.8	4.0	2.5	2.9	100
		2	3.4	3.0	3.9	3.7	3.3	
3	2 m/3 cm	1	3.1	3.6	2.8	2.3	3.8	100
		2	2.5	3.9	2.9	2.3	3.6	
4	2 m/3 cm	1	4.3	2.1	3.7	2.8	2.4	80
		2	2.9	2.2	4.0	2.7	4.5	
5	2 m/3 cm	1	3.1	2.8	3.2	2.9	3.3	80
		2	2.6	3.5	1.9	3.6	4.7	

6 Conclusions

(1) This paper focuses on the walking chassis of a self-propelled peanut planter in hilly mountainous areas. A multi-objective optimization mathematical model was established, and structural optimization of the walking chassis was performed based on the MOGA intelligent optimization algorithm to achieve the goal of lightweight chassis structure.

(2) A finite element model was established based on the dimensions of the walking chassis, and an analysis of the finite element model was conducted to provide a basis for static structural analysis and lightweight optimization design. The Latin hypercube design method and Kriging approximation model were used to simulate the response relationship between design variables and design objectives. Considering performance indicators such as the mass of the walking chassis, maximum stress, and maximum displacement, the MOGA algorithm was employed for multi-objective optimization of the walking chassis. The lightweight design effectively reduced the mass of the peanut planter chassis from the original 203-144.29 kg; the maximum deformation was 1.3997 mm. Under the premise of meeting allowable stress requirements and avoiding resonance phenomena, static stability was improved, satisfying design and usage requirements. Experiments indicate that this optimization method has a good optimization effect, effectively improving optimization efficiency and providing a reliable approach for further lightweight design of self-propelled peanut planters in hilly mountainous areas.

(3) Field test results showed that, when operating at different speeds as set by the experiment, the qualified rate of plant spacing was ≥98%, and the missed sowing rate was <1.5%. The prototype performed well at different speeds, with minimal impact on the qualified rate of plant spacing. The qualified rate for sowing depth was ≥90%, and the sowing depth remained stable. After the chassis was lightened, no issues such as reduced pass-ability or decreased stability were observed during field tests, demonstrating reliable working performance.

Acknowledgements

This work was financially supported by the National Key R&D Program Project (Grant No. 2023YFD2001002) and Shandong Peanut Industry Technology System (SDAIT-04-08).

[References]

[1] Zhao S C, Lü J L, Xu X P, Lin X M, Rosso L M, Qiu S J, et al. Peanut yield, nutrient uptake and nutrient requirements in different regions of China. Journal of Integrative Agriculture, 2021; 20(9): 2502–2511.

[2] Chen F D, Jiang J T, Wang D W, Bao Y F, Yang W Q. Current application

status and research progress of peanut planting machinery. Jiangsu Agricultural Sciences, 2020; 48(13): 41–46. (in Chinese)
[3] Gao Y, Zhang L J. Development status and countermeasures of peanut seeding mechanization in hilly and mountainous areas. Agricultural Technology & Equipment, 2024; 6: 13–15. (in Chinese)
[4] Meng X J, Zhao D, Kong L H, Cai D M. Design and analysis of planting mechanism for a self-propelled transplanting machine. Journal of Physics: Conference Series, 2021; 2010(1): 012199.
[5] Rosenthal S, Maaß F, Kamaliev M, Marlon Hahn; Gies S, Tekkaya A E. Lightweight in automotive components by forming technology. Automotive Innovation, 2020; 3(3): 195–209.
[6] Zhu R J, Li Y M, Xu L Z, Liu Y. Multi-objective optimization design of the tracked combine harvester chassis frame. Research on Agricultural Mechanization, 2023; 45(2): 36–43. (in Chinese)
[7] Yuan S L, Zhang L H, Qiu Q Y, Luo H Z. Multi-objective lightweight design of frame for crawler corn combine harvester. Journal of Hunan Agricultural University (Natural Sciences), 2023; 49(3): 371–376. (in Chinese)
[8] Tian Z J, Cheng C J, Wang B H. Structural analysis and lightweight of pickup truck frame under multiple working conditions. Automotive Components, 2022; 10: 27–34. (in Chinese)
[9] Wang F A, Cao Q Z, Li Y B, Pang Y L, Xie K T, Zhang Z G. Design and trafficability experiment of self-propelled potato harvester in hilly and mountainous areas. Transactions of the CSAM, 2023; 54(S2): 10–19. (in Chinese)
[10] Chen Y N, Xie B, Du Y F, Mao E R. Powertrain parameter matching and optimal design of dual-motor driven electric tractor. Int J Agric & Biol Eng, 2019; 12(1): 33–41.
[11] He R. Lightweight design of frame structures based on multidiscipline and multi-objective. Noise and Vibration Control, 2022; 42(2): 173. (in Chinese)
[12] Zhang J, Ran W. Lightweight optimization design of a light electric commercial vehicle frame. Journal of Physics: Conference Series, 2021; 1939(1): 012038.
[13] Yu Y, Diao L S, Wang D W, Wang J S, Wang X M, Tan X Z, et al. Lightweight design of peanut sowing machine frame based on finite element analysis. Int J Agric & Biol Eng, 2023; 16(3): 120–129.
[14] Yu C J, Z D B, Shu C S, Cao Y, Zhong Y L, Zhang C L. The improved tobacco stalk pulling and shredding machine frame lightweight design. Journal of Agricultural Mechanization Research, 2021; 43(5): 109–115. (in Chinese)
[15] Zhang X P, Wang D F, Kong D W, Huang B T, Zhang Z F, He Y. The anti-fatigue lightweight design of heavy tractor frame based on a modified decision method. Structural and Multidisciplinary Optimization, 2022; 65(10): 280.
[16] Li Y, Xu Z M, Zhang L H, Du Y, Jiang Y C. Light weight design of chassis frame for a soybean harvester. Journal of Chongqing University, 2019; 42(10): 14–21. (in Chinese)
[17] Zhang X, Xu W, Li R, et al. Study on sustainable lightweight design of airport waiting chair frame structure based on ANSYS Workbench. Sustainability, 2024; 16(13): 5350.
[18] Zhang Y, Zhang C L. Research on lightweight design of automobile structure considering uncertain variables. Journal of Lanzhou University of Technology, 2024; 5: 52–61.
[19] Kan B, Gong K J. Optimal design of novel-shaped frame of truss quadrotor UAV. Machinery Design & Manufacture, 2024; 11: 281–284. (in Chinese)
[20] Zhu H, Huang C L, Yang L M, Li J F. Optimization of quadrotor UAV frame structure based on response surface method and topology optimization. Journal of Machine Design, 2023; S2: 130–135. (in Chinese) DOI: 10.13841/j.cnki.jxsj.2023.s2.013
[21] Ye S R, Hao W Y, Sun Z, Guo X. Lightweight design method of transmission frame structure considering the overhang constraint of additive manufacturing. Journal of Rocket Propulsion, 2023; 49(4): 26–35, 123. (in Chinese)
[22] Zhao C Z, Zhang C L, Li Y, Bo C Z, Hao G F, Dou H B. Design and optimization of the frame of the air-driven electrostatic spray locomotive. Journal of Physics: Conference Series, 2020; 1650(2): 022057.
[23] Li Y F, Li C. Topology optimization and simulation of compression-shear test machine frame. Machine Tool & Hydraulics, 2023; 5: 189–195. (in Chinese)
[24] Huang D W, Guo C R, Fu A J, Tian Y K, Gong Y X. Optimization design of the carriage frame of a livestock and poultry transport vehicle based on multiple working conditions. Journal of Chinese Agricultural Mechanization, 2023; 44(10): 137–143.
[25] Feng Y L, Yin X C, Jin H R, Tong W Y, Ning X F. Design and experiment of a Chinese chive harvester. Int J Agric & Biol Eng, 2023; 16(2): 125–131.
[26] Tang H, Xu C, Zhu J, et al. Vibration analysis and topology optimization of the header of full-feeding rice combine harvester. Int J Agric & Biol Eng, 2023; 16(4): 96–108.
[27] Chen K K, Yuan Y W, Zhao B, Jin X, Lin Y, Zheng Y J. Finite element modal analysis and experiment of rice transplanter chassis. Int J Agric & Biol Eng, 2022; 15(5): 91–100.
[28] Jin X, Chen K, Ji J, et al. Intelligent vibration detection and control system of agricultural machinery engine. Measurement, 2019; 145: 503–510.
[29] Jin X, Cheng Q, Tang Q, Wu J, Jiang L, Wu C Y, et al. Research on vibration reduction test and frame modal analysis of rice transplanter based on vibration evaluation. Int J Agric & Biol Eng, 2022; 15(4): 116–122.
[30] Ma Y H, Wang X C, Zuo W J. Analytical sensitivity analysis method of cross-sectional shape for thin-walled automobile frame considering global performances. International Journal of Automotive Technology, 2020; 21(5): 1207–1216.
[31] Wang Q Q, Li Z D, Wang W W, Zhang C L, Chen L Q, Wan L. Multi-objective optimization design of wheat centralized seed feeding device based on particle swarm optimization (PSO) algorithm. Int J Agric & Biol Eng, 2020; 13(6): 76–84.
[32] Hua Y Z, Zhu H Q, Gao M, Ji Z Y. Multi-objective optimization design of permanent magnet assisted bearing less synchronous reluctance motor using NSGA-Ⅱ. IEEE Transactions on Industrial Electronics, 2021; 68(11): 10477–10487.
[33] Chen Y, Mao E R, Li W, Zhang S, Song Z H, Yang S J, et al. Design and experiment of a high-clearance self-propelled sprayer chassis. Int J Agric & Biol Eng, 2020; 13(2): 71–80.